Scalar wave scattering in spherical cavity resonator with conical channels

Hipolito Garcia-Gracia* and Julio C. Gutiérrez-Vega

Photonics and Mathematical Optics Group, Tecnológico de Monterrey, Monterrey 64849, Mexico
**Corresponding author: hgarciag@itesm.mx*

Received October 29, 2013; accepted November 27, 2013;
posted December 12, 2013 (Doc. ID 200326); published January 9, 2014

We study the scalar wave scattering off the spherical cavity resonator with two finite-length conical channels attached. We use the boundary wall method to explore the response of the system to changes in control parameters, such as the size of the structure and the angular width of the input and output channels, as well as their relative angular position. We found that the system is more sensitive to changes in the input channel, and a standing wave phase distribution occurs within the cavity for nontransmitting values of the incident wave number. We also saw that an optical vortex can travel unaffected through the system with aligned channels.

OCIS codes: (290.5825) Scattering theory; (240.3695) Linear and nonlinear light scattering from surfaces.
http://dx.doi.org/10.1364/JOSAA.31.000246

1. INTRODUCTION

Hollow resonators are a useful tool to study more complex optical and acoustical resonating structures. Thanks to modern fabrication techniques, it is now possible to build resonator-like structures on smaller scales than ever, in the range of nanometers, where classical mechanics fail and the quantum nature of the system must be considered. Since quantum mechanics gives us a wave-based description of the subatomic world, wave resonators can be used as a tool to explore the properties of such quantum-scale objects, and so the study of quantum billiards and wave resonators is now linked to one another. Two-dimensional resonators are the most popular type of resonators since they allow us to analyze the behavior of systems that have a translational symmetry such as wave guides and fibers, or those in which the third dimension is so small it allows no oscillations normal to the transverse plane to occur, such as quantum corrals formed by a single line of atoms deposited along a closed path on a substrate. Thus, the study of two-dimensional billiards has been focused on exploring different possible geometries, such as rectangular and circular [1,2], and more complicated geometries like the hexagonal [3], elliptic [4–6], and parabolic [7] systems. Three-dimensional (3D) cavities are also popular among classical and quantum chaos researchers, and several different geometries have been studied, such as the perturbed spherical [8–10], generalized stadium [11], conical [12], prolate spheroidal [13], ellipsoidal [14], and Sinai billiards [15], among others.

Wave scattering and transport through open resonating structures has been another active area of research, since such systems can be used to model quantum dots with border imperfections or leakage, as well as open nano-resonators. The transport properties of several open 2D cavity structures have been studied recently, including the rectangular [16,17], circular [18–21], stadium [22,23], and elliptic billiards [24]. However, open 3D cavities have not received quite as much attention as their two-dimensional counterparts, and to the best of our knowledge, there is no work regarding the scattering properties of the spherical resonator with attached channels.

This work focuses on studying the wave scattering and transport properties of the open spherical resonator with two finite-length conical channels as an example of a 3D open system. We explore the response of the system to variations in size, the angular width of the input and output channels, and the relative angular position of the channels.

2. OPEN SPHERICAL RESONATOR

The open spherical resonator is shown in Fig. 1. The system consists of a spherical cavity of radius r_0, with two conical leads, input and output, connected to it. The cones that form the input and output channels begin at r_0 and extend up to a radius of $2r_0$. The input cone has its axis along $\theta = 0$, where θ is the spherical polar angle, and has an angular half-width of $\Delta\theta_{\text{in}}$. The output cone is centered at the polar angle θ_{out} and has a angular half-width of $\Delta\theta_{\text{out}}$. We fix the angular position of the output cone to $\theta_{\text{out}} = \pi$ and the angular half-widths of the channels to $\Delta\theta_{\text{in}} = \Delta\theta_{\text{out}} = \pi/8$, except when we study the response of the system to changes in these parameters. Without any loss of generality, the incoming wave is always incident on the cone along the positive z axis. Since the system is reminiscent of quantum billiard structures, we use the terms *billiard* and *resonator* indistinctively, since we are studying an open resonator that can also function as a 3D quantum billiard.

In order to observe how the behavior of the resonator changes due to parameter variations, we use input and output profiles, I_{in} and I_{out}, respectively. To generate these profiles, first we calculate the full scattering wave function $\psi(\mathbf{r})$ using the boundary wall method, which includes the incident wave and the scattered solution inside the system. Then the profiles are obtained by numerically integrating $|\psi(\mathbf{r})|^2$ over the

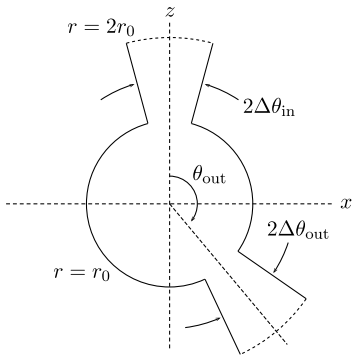

Fig. 1. Transverse cut of the open spherical quantum billiard on the $y = 0$ plane.

volume of the input and output channels, respectively. Appendix A gives a brief description of the boundary wall method, and for a more detailed definition we refer the reader to the works by da Luz *et al.* [25] and Zanetti *et al.* [26,27].

The boundary wall method does not specify the incident wave $\phi(\mathbf{r})$ to be used for the calculations of the wave function $\psi(\mathbf{r})$, so long as $\phi(\mathbf{r})$ is a solution of

$$H_0(\mathbf{r})\phi(\mathbf{r}) = E\phi(\mathbf{r}), \tag{1}$$

where $H_0(\mathbf{r})$ is the free-space Hamiltonian. The general solution of Eq. (1) can be written as a linear superposition of plane waves, so for simplicity we set

$$\phi(\mathbf{r}) = \exp[ik(x\cos\varphi\sin\theta + y\sin\varphi\sin\theta + z\cos\theta)]. \tag{2}$$

Since the incoming wave is always incident on the cone along the positive z axis, its propagation vector must point along the negative z axis, which is specified by setting $\theta = \pi$ and reduces Eq. (2) to

$$\phi(\mathbf{r}) = \exp(-ikz), \tag{3}$$

where k is the wave number of the incident plane wave. We use normalized units for r_0 and k, which can be converted to a desired physical dimension by simple linear transformations.

A. Scaling

To study the response of the system to changes in size, we vary the radius of the spherical cavity r_0, which scales the structure accordingly. Figure 2 shows the input and output profiles as a function of the wave number k of the incident plane wave for radii $r_0 = \{0.75, 1.00, 1.25\}$. We know that the energies of the spherical infinite potential well scale as $1/r_0^2$, and we use our numerical data to verify that the open spherical quantum billiard inherits this property. First let us consider the first maximum for each of the input profiles in Fig. 2(a), where we have

$$k_{0.75} = 5.858, \qquad k_{1.00} = 4.395, \qquad k_{1.25} = 3.513,$$

and compare the squared ratios $(k_{0.75}/k_{1.00})^2$ and $(k_{1.00}/k_{1.25})^2$ with the corresponding inverse squared ratios of radii to get

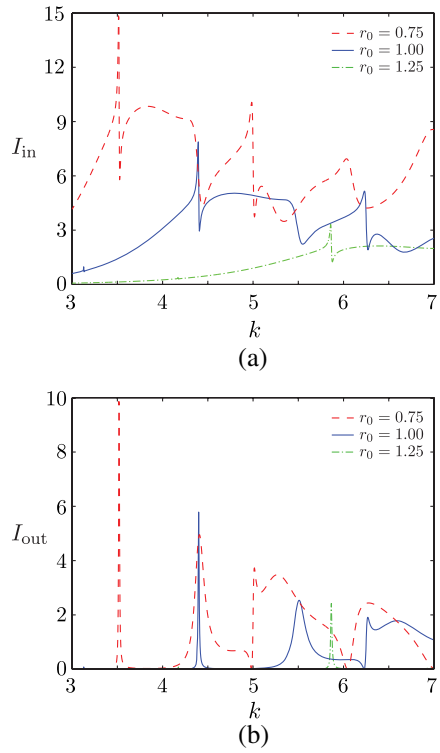

Fig. 2. Input and output profiles as a function of the wave number k for spherical cavity radii $r_0 = \{0.75, 1.00, 1.25\}$.

$$\left(\frac{k_{0.75}}{k_{1.00}}\right)^2 = 1.7766 \quad \text{and} \quad \left(\frac{1.00}{0.75}\right)^2 = 1.7778,$$
$$\left(\frac{k_{1.00}}{k_{1.25}}\right)^2 = 1.5650 \quad \text{and} \quad \left(\frac{1.25}{1.00}\right)^2 = 1.5625. \tag{4}$$

To check whether the scaling holds for I_{out}, we consider the first maximum for each of the output profiles in Fig. 2(b), where we have

$$k_{0.75} = 5.866, \qquad k_{1.00} = 4.399, \qquad k_{1.25} = 3.518.$$

We compare the same squared ratios $(k_{0.75}/k_{1.00})^2$ and $(k_{1.00}/k_{1.25})^2$ with their corresponding inverse squared ratios of radii to get

$$\left(\frac{k_{0.75}}{k_{1.00}}\right)^2 = 1.7782 \quad \text{and} \quad \left(\frac{1.00}{0.75}\right)^2 = 1.7778,$$
$$\left(\frac{k_{1.00}}{k_{1.25}}\right)^2 = 1.5636 \quad \text{and} \quad \left(\frac{1.25}{1.00}\right)^2 = 1.5625. \tag{5}$$

We can see from Eqs. (4) and (5) that the scaling factor of $1/r_0^2$ is indeed inherited by the open spherical resonator after attaching the conical channels. Furthermore, we would also expect the entire profile to scale itself such that for a larger cavity radius the difference in *energy* between two profile features is compressed by the same factor. To verify this we use the first two maxima of the output profiles for $r_0 = \{1.00, 1.25\}$, and we consider the difference of squared wave numbers $\Delta k^2 = k_2^2 - k_1^2$. From our numerical data we have

$$\Delta k^2_{1.00} = 10.9999 \quad \text{and} \quad \Delta k^2_{1.25} = 7.0505$$

and their ratio gives $(\Delta k^2_{1.00}/\Delta k^2_{1.25}) = 1.5602$, which is comparable to the squared ratio of radii $(1.25/1.00)^2 = 1.5625$, thus proving that the difference in energies is also scaled by $1/r_0^2$ in our system.

B. Angular Half-Width

Next we study the response of the system to changes in the angular half-width of the input and output channel. To do this, we fix the radius of the spherical cavity of $r_0 = 1$ and we observe the behavior of the output profile I_{out} as we vary one of the angular half-widths at a time. Figure 3 shows the output profile for $\Delta\theta_{\text{in}} = \{3\pi/32, 4\pi/32, 5\pi/32, 6\pi/32\}$ and the wave numbers $k_{n,l} = \sqrt{E_{n,l}}$ corresponding to the first four eigenenergies $E_{n,l}$ of the traditional spherical quantum billiard as reference, where n and l are the radial and polar quantum numbers, respectively. We can see from Fig. 3 that for small apertures the output profile is almost nonexistent, which is due to the fact that for small apertures there needs to be a sufficiently small wavelength (sufficiently large wave number) of the incident wave in order to have enough energy enter the system to produce an output. Furthermore, as we increase the width of the input channel, we see some spikes at lower values of k near the $k_{n,l}$ of the closed billiard, which indicates there are resonance phenomena occurring within the spherical cavity of the system, producing sudden outbursts of energy through the output channel. We can also see smooth features at higher values of k, which in turn appear at decreasingly lower values of the wave number for wider input channel configurations.

On the other hand, Fig. 4 shows I_{out} for $r_0 = 1$ and $\Delta\theta_{\text{out}} = \{3\pi/32, 4\pi/32, 5\pi/32, 6\pi/32\}$, as well as the first four $k_{n,l}$ of the spherical infinite potential well. We can see from Fig. 4 that for a fixed input aperture, the amount of energy entering the resonator is constant, so by increasing the width of the output channel we distribute that energy a longer range of k, which can be seen in the diminishing maxima of the profiles as they spread over longer ranges of wave numbers. Furthermore, we can see that there must be an optimal value of the output width, since the profile is rather low for $\Delta\theta_{\text{out}} = 3\pi/32$, then increases to a maximal distribution for $\Delta\theta_{\text{out}} = 4\pi/32$ and then decreases again for $\Delta\theta_{\text{out}} = \{5\pi/32, 6\pi/32\}$. We can conclude that variations in the width of the input channel have a global effect on the transport through the system, since they control the amount of energy actually entering the resonator, whereas changes in the output width have a local effect on the features in the profile, since they control how the existing energy within the cavity is expelled without adding or removing additional energy from it. Furthermore, there seems to be an optimal value of the output channel width for a corresponding input channel width that maximizes the tunneling through the system.

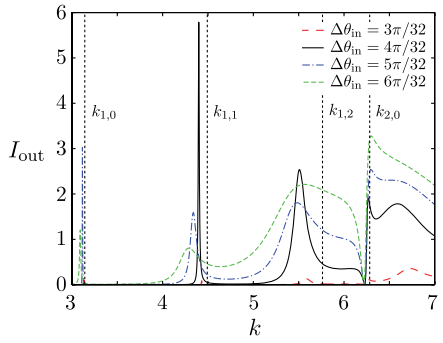

Fig. 3. Output profile I_{out} as a function of the wave number k for different values of the angular half-width of the input channel $\Delta\theta_{\text{in}}$. The black vertical dotted lines indicate the wave numbers $k_{n,l}$ for the first four eigenenergies $E_{n,l}$ of the traditional spherical quantum billiard of radius $r_0 = 1$.

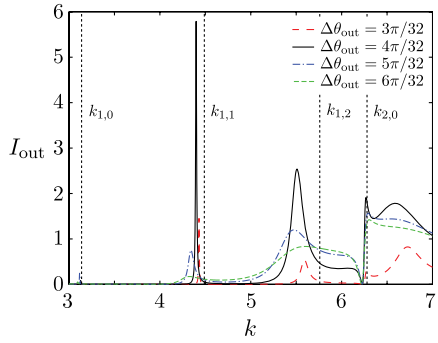

Fig. 4. Output profile I_{out} as a function of the wave number k for different values of the angular half-width of the output channel $\Delta\theta_{\text{out}}$. The black vertical dotted lines indicate the wave numbers $k_{n,l}$ for the first four eigenenergies $E_{n,l}$ of the traditional spherical quantum billiard of radius $r_0 = 1$.

C. Relative Angular Positions

Finally, we study the effect of varying the relative difference in angular position between the input and output channel. To do this we take advantage of the symmetry properties of the spherical coordinate system, so without any loss of generality we need only change the angular position of the output lead θ_{out}, since any other configuration with the same relative difference in positions can be obtained by simple rotation operations.

Figure 5 shows the input and output profiles for different values of the output angular position θ_{out}. We can see in Fig. 5(a) that changing the angular position of the output channel has virtually no effect up to $k_0 = 5.3607$, which seems to be the value of the wave number k where the energy of the incident wave begins to cause significant changes in the resonance characteristics of the cavity. For $k > k_0$, the input profile I_{in} is more sensitive to variations in θ_{out} since the wave function $\psi(\mathbf{r})$ changes within the spherical cavity and this in turn modifies the amount of energy, which is reflected by the system.

Furthermore, we can see in Fig. 5(b) that the output profile I_{out} is also quite insensitive to changes in θ_{out} for $k < k_0$, which confirms that the resonance phenomena within the cavity is relatively unaffected by the incident wave within that range of k. For $k > k_0$, the output profile varies prominently with changes in θ_{out}, which is due to the fact that by changing the angular position of the output channel, we partially include or exclude different maxima and minima of the wave function $\psi(\mathbf{r})$ near $r = r_0$ resulting from the superposition of the different degenerate eigenstates associated with nearby $k_{n,l}$, which in turns alters how the energy exits the system through the output cone. If we consider the output profile near $k_{1,2}$, we can see that the profile varies both in amplitude and in the position of the maximum in k, which is very

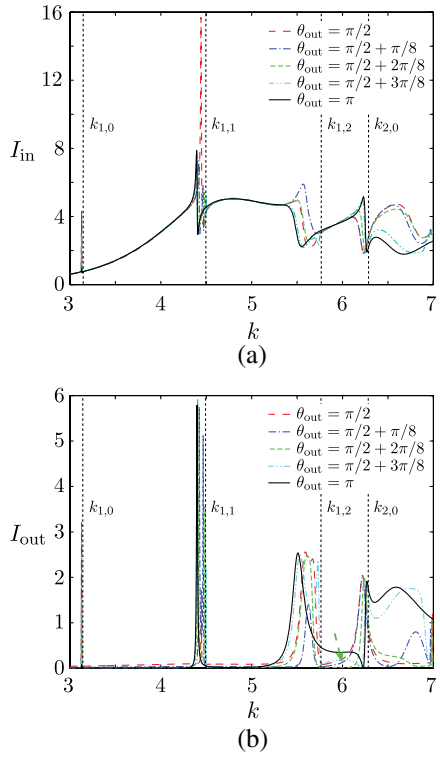

Fig. 5. Input and output profile as a function of the wave number k for different values of the angular position of the output channel θ_{out}. The black vertical dotted lines indicate the wave numbers $k_{n,l}$ for the first four eigenenergies $E_{n,l}$ of the traditional spherical quantum billiard of radius $r_0 = 1$.

likely caused by how the maxima and minima of the wave function are distributed for the generated superposition of eigenstates $k_{1,2}$. We recall that for $l = 2$ such a superposition would contain $m = 2l + 1 = 5$ different energy-degenerate eigenstates, corresponding to the third quantum number $m = \{-2, -1, 0, +1, +2\}$.

Figure 6 shows a transverse cut at $y = 0$ of the amplitude $|\psi(\mathbf{r})|$ and phase $\Phi(\mathbf{r})$ of the wave function $\psi(\mathbf{r})$ for an angular position $\theta_{\text{out}} = \pi/2 + 2\pi/8$ of the output channel and an incident wave number $k = 6.00$, which corresponds to the point of no transmission indicated in Fig. 5(b). We can clearly see that, for the combination of parameters that inhibits the transmission through the system, there is a discontinuous phase distribution inside the spherical cavity that indicates

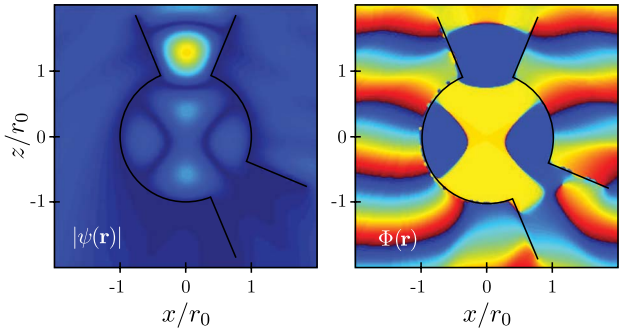

Fig. 6. Transverse cut at $y = 0$ of the amplitude $|\psi(\mathbf{r})|$ and phase $\Phi(\mathbf{r})$ of the wave scattered by the open spherical resonator with $\theta_2 = \pi/2 + 2\pi/8$ and an incident wave with wave number $k = 6.00$ corresponding to the minimum indicated in Fig. 5(b).

a standing wave phenomenon is occurring within the resonator. We can also observe that the output channel presents a phase singularity that can only occur when both the real and imaginary parts of the wave function are zero, which supports the fact that there is no outgoing energy exiting through the output cone.

To study a purely 3D phenomenon in the open spherical resonator, we modified the incident wave to generate a beam carrying orbital angular momentum (OAM) of charge L and observe how the beam propagates through the system. The incident beam with OAM charge L can be written as a superposition of N plane waves evenly distributed along a cone given by a polar angle θ,

$$\phi(\mathbf{r}) = \sum_{j=0}^{N-1} \exp(iL\varphi_j) \times \exp[ik(x \cos\varphi_j \sin\theta + y \sin\varphi_j \sin\theta + z \cos\theta)], \tag{6}$$

where $\varphi_j = 2\pi j/N$.

As an example of the propagation of a beam carrying OAM through the billiard, we use a beam with $L = 1$ constructed from a superposition of $N = 20$ plane waves evenly distributed along the cone generated by the polar angle $\theta = \pi/5$, and we observe how the beam propagates through an azimuthally symmetric system obtained by setting $\theta_{\text{out}} = \pi$, and an asymmetric system where the output channel is centered at $\theta_{\text{out}} = \pi/2 + \pi/3$. The values of k and θ were chosen such that the first off-axis zero of the beam matched the smallest aperture of the input cone.

Figure 7 shows the amplitude $|\psi(\mathbf{r})|$ and phase $\Phi(\mathbf{r})$ of the wave function at transverse planes $y = 0$ and $z = 0$ for the azimuthally symmetric billiard with $\theta_{\text{out}} = \pi$, whereas Fig. 8

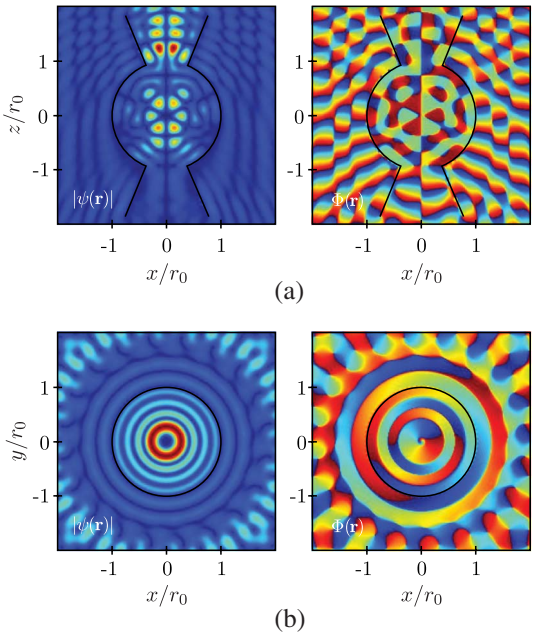

Fig. 7. Transverse cut at (a) $y = 0$ and (b) $z = 0$ of the amplitude $|\psi(\mathbf{r})|$ and phase $\Phi(\mathbf{r})$ of the wave function generated by the open spherical quantum billiard with $\theta_2 = \pi$ and an incident beam with wave number $k = 17.00$ carrying OAM $L = 1$, formed by 20 plane waves incident along a cone of $\theta = \pi/5$.

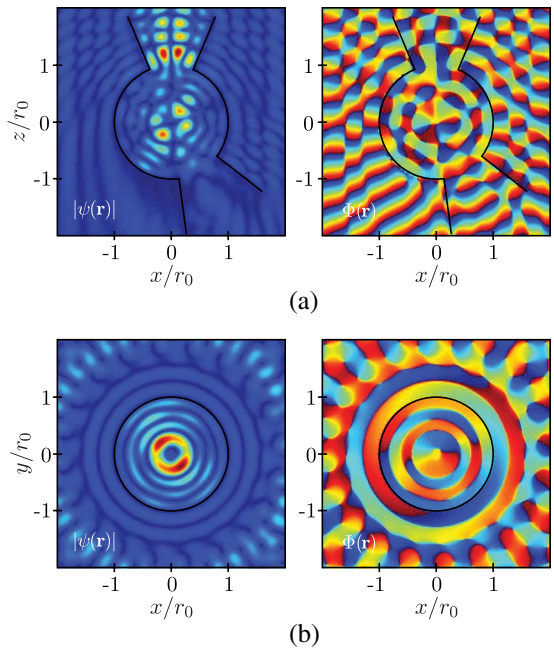

Fig. 8. Transverse cut at (a) $y = 0$ and (b) $z = 0$ of the amplitude $|\psi(\mathbf{r})|$ and phase $\Phi(\mathbf{r})$ of the wave function generated by the open spherical quantum billiard with $\theta_2 = \pi/2 + \pi/3$ and an incident beam with wave number $k = 17.00$ carrying OAM $L = 1$, formed by 20 plane waves incident along a cone of $\theta = \pi/5$.

does so for the asymmetric billiard with $\theta_{\text{out}} = \pi/2 + \pi/3$. We can see from Fig. 7(a) that the central vortex is maintained during propagation through the system, regardless of the reflection and diffraction phenomena that occurs within the billiard. Furthermore, Fig. 7(b) shows that the symmetry of the beam is preserved within the system. In contrast, we can easily observe in Figs. 8(a) and 8(b) that once the azimuthal symmetry of the system is broken, the central vortex is unable to travel intact through the system as it generates multiple creation-annihilation events within the billiard cavity, which also disrupts the transverse symmetry of the beam.

3. CONCLUSIONS

In this work we studied the scattering properties of the open spherical resonator with finite-length conical channels. To characterize the transmission through the system, we analyzed the effect introduced by variations in the size of the billiard cavity, the angular aperture of the input and output channels, and the relative difference in angular positions between the leads.

We found that after attaching the channels, the system roughly retained the $1/r_0^2$ scaling property that is present in the eigenenergies of the spherical infinite well: the square of the wave number k corresponding to a particular feature in the input or output profile scaled as the inverse squared radius of the spherical cavity, and the difference of squared wave numbers $k_2^2 - k_1^2$ corresponding to two given features within the profile also had the same scaling factor. We also studied the effect of varying the angular width of the channels on the output profile of the system. First we changed the angular aperture of the input channel and we saw that for smaller apertures there was not enough energy entering the system to produce transmission through the system, and as we increased the aperture, we observed resonance spikes at lower values of k and smoother transmission for higher values of k, which started at lower wave numbers for wider input channels due to a larger amount of energy traveling through the system. On the other hand, we saw that widening the output channel caused the profile to become smoother as the sharp features were distributed over wider ranges of wave numbers. We also observed that for a given input channel configuration, there is an optimal output width that enhances transmission peaks near resonance. Finally, we studied the effect of displacing one of the channels from the default aligned position, and we found that for k below a certain threshold value the system was not very sensitive but this sensitivity increased for wave numbers greater than the threshold value. In addition to this, the input profile was less sensitive than the output profiles to variations in the angular position of the output channel. Also, when a beam with an optical vortex along its propagation axis goes through the system, the optical vortex travels through unaffected when the channels are aligned, but it breaks up and experiences multiple creation-annihilation events when the symmetry of the system is broken.

The boundary wall method gives the steady state wave function for a particular combination of incident wave and scattering structure. For a more profound characterization of the open spherical resonator, we would explore a real-time solution method such as finding the wave function as a superposition of time-varying orthogonal modes inside the spherical cavity and the conical channels and study the behavior of the expansion coefficients as we vary the different parameters. We also wish to analyze the semiclassical aspects of the system by considering wavelengths much smaller than the dimensions of the system, placing us in the ballistic regime of the problem, which may exhibit some very interesting tunneling properties comparable to classical trajectories of free particles inside the system.

APPENDIX A: BOUNDARY WALL METHOD

Here we briefly define the boundary wall method used throughout this paper. Let us consider the time-independent Schrödinger equation $H(\mathbf{r})\psi(\mathbf{r}) = E\psi(\mathbf{r})$, with $H(\mathbf{r}) = H_0(\mathbf{r}) + V(\mathbf{r})$, and E the energy of the Hamiltonian $H(\mathbf{r})$. The solution for $\psi(\mathbf{r})$ can be obtained from Green's function method, and is given by

$$\psi(\mathbf{r}) = \phi(\mathbf{r}) + \int d\mathbf{r}' G_0(\mathbf{r}, \mathbf{r}') V(\mathbf{r}')\psi(\mathbf{r}'), \tag{A1}$$

where $\phi(\mathbf{r})$ solves $H_0(\mathbf{r})\phi(\mathbf{r}) = E\phi(\mathbf{r})$ and $G_0(\mathbf{r}, \mathbf{r}')$ is the Green's function for H_0. Now we introduce a δ-type potential given by

$$V(\mathbf{r}) = \gamma \int_{\mathcal{C}} ds \delta(\mathbf{r} - \mathbf{r}(s)), \tag{A2}$$

where the integral is done over the boundary $\mathcal{C}$, which can be open or closed, connected or disconnected. Here $\mathbf{r}(s)$ is the position vector of the point s on the boundary $\mathcal{C}$ and the set of all such vectors is called $\mathcal{S}$, and γ is known as the strength of the potential. It is easy to see that $V(\mathbf{r}) = 0$ for any $\mathbf{r}$ that does not belong to $\mathcal{S}$. When $\gamma \to \infty$, the wave

function will satisfy the Dirichlet boundary condition and vanish at the boundary $\mathcal{C}$. For finite values of γ the boundary behaves as a finite potential wall, and some penetration of the wave function is possible.

If we insert the δ-type potential in Eq. (A2) into Eq. (A1), we can perform the integral trivially thanks to the delta function; thus we obtain

$$\psi(\mathbf{r}) = \phi(\mathbf{r}) + \gamma \int_{\mathcal{C}} ds' G_0(\mathbf{r}, \mathbf{r}(s'))\psi(\mathbf{r}(s')), \tag{A3}$$

and setting $\gamma\psi(\mathbf{r}(s)) = T_\phi(\mathbf{r}(s))$ we get

$$\psi(\mathbf{r}) = \phi(\mathbf{r}) + \int_{\mathcal{C}} ds' G_0(\mathbf{r}, \mathbf{r}(s'))T_\phi(\mathbf{r}(s')). \tag{A4}$$

From Eq. (A4) we can clearly see that if $T_\phi(\mathbf{r}(s))$ is known for all points s on the boundary $\mathcal{C}$, then the wave function at any point $\mathbf{r}$ can be obtained by a single definite integral. If we let $\mathbf{r} = \mathbf{r}(s'')$ be some point on $\mathcal{S}$, then Eq. (A3) becomes

$$\psi(\mathbf{r}(s'')) = \phi(\mathbf{r}(s'')) + \gamma \int_{\mathcal{C}} ds' G_0(\mathbf{r}(s''), \mathbf{r}(s'))\psi(\mathbf{r}(s')). \tag{A5}$$

Equation (A5) can be formally solved in matrix form, which gives

$$\tilde{\psi} = [\tilde{I} - \gamma\tilde{G}_0]^{-1}\tilde{\phi}, \tag{A6}$$

where $\tilde{\psi}$ and $\tilde{\phi}$ stand for the vectors of $\psi(\mathbf{r}(s))$'s and $\phi(\mathbf{r}(s))$'s on the boundary, and $\tilde{I}$ is the identity operator. The tildes indicate that all functions and vectors are evaluated exclusively on the boundary $\mathcal{C}$.

If we define the T operator as

$$T = \gamma[\tilde{I} - \gamma\tilde{G}_0]^{-1}, \tag{A7}$$

then it is clear from Eqs. (A6) and (A7) that T_ϕ in Eq. (A4) is given by

$$T_\phi(\mathbf{r}(s')) = \int ds T(\mathbf{r}(s'), \mathbf{r}(s))\phi(\mathbf{r}(s)). \tag{A8}$$

Finally, using $\gamma\psi(\mathbf{r}(s)) = T_\phi(\mathbf{r}(s))$ and Eq. (A8), we can rewrite Eq. (A5) as

$$\tilde{\psi} = [\tilde{I} + \tilde{G}_0 T]\tilde{\phi}. \tag{A9}$$

Since calculating the analytical form of $\psi(\mathbf{r})$ is not always possible for most cases, sometimes we need to solve the problem numerically. We divide the boundary $\mathcal{C}$ into N segments C_j, for $j = 1 \ldots N$. Let $\mathbf{r}(s)$ be a point on the boundary; we can approximate the wave function $\psi(\mathbf{r})$ as

$$\begin{aligned}\psi(\mathbf{r}) &= \phi(\mathbf{r}) + \sum_{j=1}^{N} \int_{C_j} ds\gamma G_0(\mathbf{r}, \mathbf{r}(s))\psi(\mathbf{r}(s)),\\ &\approx \phi(\mathbf{r}) + \sum_{j=1}^{N} \psi(\mathbf{r}(s_j)) \int_{C_j} ds\gamma G_0(\mathbf{r}, \mathbf{r}(s)),\end{aligned} \tag{A10}$$

where s_j is the middle point of segment C_j. For simplicity we abbreviate $\mathbf{r}_j = \mathbf{r}(s_j)$. If we consider $\mathbf{r} = \mathbf{r}_i$ some other point on $\mathcal{C}$, we can rewrite Eq. (A10) as

$$\psi(\mathbf{r}_i) = \phi(\mathbf{r}_i) + \sum_{j=1}^{N} \gamma M_{ij}\psi(\mathbf{r}_i), \tag{A11}$$

where

$$M_{ij} = \int_{C_j} ds G_0(\mathbf{r}_i, \mathbf{r}(s)). \tag{A12}$$

Throughout this work, we perform the segment integrals for M_{ij} with the Gauss–Legendre quadrature method in order to minimize error and the number of integration points required for each segment.

Let $\Psi = [\psi(\mathbf{r}_1), \ldots, \psi(\mathbf{r}_N)]^T$ be the vector of the wave function $\psi(\mathbf{r})$ evaluated at points $[\mathbf{r}_i, \ldots, \mathbf{r}_N]$ on the boundary, and $\Phi = [\phi(\mathbf{r}_1), \ldots, \phi(\mathbf{r}_N)]^T$ the vector of the incoming wave $\phi(\mathbf{r})$ also evaluated on $\mathcal{C}$. We can write Eq. (A11) in a purely matrix form, $\Psi = \Phi + \gamma\mathbf{M}\Psi$, and solve for the total wave function Ψ on the boundary

$$\gamma\Psi_i = (\mathbf{T}\Phi)_i = \gamma \sum_{j=1}^{N} [(\mathbf{I} - \gamma\mathbf{M})^{-1}]_{ij}\Phi_j, \tag{A13}$$

where $\mathbf{T} = \gamma(\mathbf{I} - \gamma\mathbf{M})^{-1}$. Now we can calculate the wave function $\psi(\mathbf{r})$ elsewhere as

$$\psi(\mathbf{r}) = \phi(\mathbf{r}) + \sum_{j=1}^{N} G_0(\mathbf{r}, \mathbf{r}_j)\Delta_j(\mathbf{T}\Phi)_j, \tag{A14}$$

where we used the mean value approximation for the last integral in Eq. (A11) and defined Δ_j as the length of the boundary segment C_j.

ACKNOWLEDGMENTS

We acknowledge support from the Consejo Nacional de Ciencia y Tecnología (Grant 182005), and from the Tecnológico de Monterrey (Grant CAT141).

REFERENCES

1. M. V. Berry, "Regularity and chaos in classical mechanics, illustrated by three deformations of a circular 'billiard'," Eur. J. Phys. **2**, 91–102 (1981).
2. R. W. Robinett, "Visualizing classical periodic orbits from the quantum energy spectrum via the Fourier transform: simple infinite well examples," Am. J. Phys. **65**, 1167 (1997).
3. R. L. Liboff and J. Greenberg, "The hexagon quantum billiard," J. Stat. Phys. **105**, 389–402 (2001).
4. H. Waalkens, J. Wiersig, and H. R. Dullin, "Elliptic quantum billiard," Ann. Phys. **260**, 50–90 (1997).
5. J. C. Gutiérrez-Vega, S. Chávez-Cerda, and R. M. Rodríguez-Dagnino, "Probability distributions in classical and quantum elliptic billiards," Rev. Mex. Fis. **47**, 480–488 (2001).
6. M. A. Bandres and J. C. Gutiérrez-Vega, "Classical solutions for a free particle in a confocal elliptic billiard," Am. J. Phys. **72**, 810 (2004).
7. R. J. Noriega-Manez and J. C. Gutiérrez-Vega, "Mode structure and attenuation characteristics of hollow parabolic waveguides," J. Opt. Soc. Am. B **24**, 2273–2278 (2007).
8. T. Prosen, "Quantization of a generic chaotic 3D billiard with smooth boundary. I. Energy level statistics," Phys. Lett. A **233**, 323–331 (1997).

9. T. Prosen, "Quantization of generic chaotic 3D billiard with smooth boundary. II. Structure of high-lying eigenstates," Phys. Lett. A **233**, 332–342 (1997).
10. İ. M. Erhan and H. Taşeli, "A model for the computation of quantum billiards with arbitrary shapes," J. Comput. Appl. Math. **194**, 227–244 (2006).
11. T. Papenbrock, "Numerical study of a three-dimensional generalized stadium billiard," Phys. Rev. E **61**, 4626–4628 (2000).
12. R. L. Liboff, "Conical quantum billiard," Lett. Math. Phys. **42**, 389–391 (1997).
13. İ. M. Erhan, "Eigenvalue computation of prolate spheroidal quantum billiard," Int. J. Math. Comput. Sci. **6**, 108–113 (2010).
14. H. Waalkens, J. Wiersig, and H. R. Dullin, "Triaxial ellipsoidal quantum billiards," Ann. Phys. **276**, 64–110 (1999).
15. H. Primack and U. Smilansky, "Quantization of the three-dimensional Sinai billiard," Phys. Rev. Lett. **74**, 4831–4834 (1995).
16. K. Na and L. E. Reichl, "Electron conductance and lifetimes in a ballistic electron waveguide," J. Stat. Phys. **92**, 519–542 (1998).
17. M. G. A. Crawford and P. W. Brouwer, "Density of proper delay times in chaotic and integrable quantum billiards," Phys. Rev. E **65**, 026221 (2002).
18. C. D. Schwieters, J. A. Alford, and J. B. Delos, "Semiclassical scattering in a circular semiconductor microstructure," Phys. Rev. B **54**, 10652–10668 (1996).
19. S. Ree and L. E. Reichl, "Aharonov–Bohm effect and resonances in the circular quantum billiard with two leads," Phys. Rev. B **59**, 8163–8169 (1999).
20. K. Fuchss, S. Ree, and L. E. Reichl, "Scattering properties of a cut-circle billiard waveguide with two conical leads," Phys. Rev. E **63**, 016214 (2000).
21. I. Březinová, L. Wirtz, S. Rotter, C. Stampfer, and J. Burgdörfer, "Transport through open quantum dots: making semiclassics quantitative," Phys. Rev. B **81**, 125308 (2010).
22. H. Ishio, "Quantum transport and classical dynamics in open billiards," J. Stat. Phys. **83**, 203–214 (1996).
23. C. P. Dettmann and O. Georgiou, "Transmission and reflection in the stadium billiard: time-dependent asymmetric transport," Phys. Rev. E **83**, 036212 (2011).
24. H. Garcia-Gracia and J. C. Gutiérrez-Vega, "Tunneling phenomena in the open elliptic quantum billiard," Phys. Rev. E **86**, 016210 (2012).
25. M. G. E. da Luz, A. S. Lupu-Sax, and E. J. Heller, "Quantum scattering from arbitrary boundaries," Phys. Rev. E **56**, 2496–2507 (1997).
26. F. M. Zanetti, E. Vicentini, and M. G. E. da Luz, "Eigenstates and scattering solutions for billiard problems: a boundary wall approach," Ann. Phys. **323**, 1644–1676 (2008).
27. F. M. Zanetti, M. L. Lyra, F. A. B. F. de Moura, and M. G. E. da Luz, "Resonant scattering states in 2D nanostructured waveguides: a boundary wall approach," J. Phys. B At. Mol. Opt. Phys. **42**, 025402 (2009).